photonics

MDPI

Article

SOA-MZI Differential Transformation Approach Applied on Simultaneous Electro-Optical Mixing

Hassan Termos [1,*] and Ali Mansour [2]

[1] ICFO—The Institute of Photonic Sciences, 08860 Barcelona, Spain
[2] Lab-STICC, CNRS UMR 6285, ENSTA Bretagne, 2 Rue François Verny, CEDEX 09, 29806 Brest, France
* Correspondence: hassan.termos@icfo.eu

Abstract: We experimentally incubate a ground-breaking design, for the first time, of concurrent electro-optical semiconductor optical amplifier Mach–Zehnder interferometer mixing (SOA-MZI) based on a differential transformation methodology. Projecting the simultaneous electro-optical mixing system and improving its efficiency and quality achievement in optical and electrical features is a crucial task due to the characteristics of an optical pulse source (OPS) operating with a repetition rate of $f = 58.5$ GHz and a pulse width duration of 1 picosecond (ps). The resultant of the contemporaneous electro-optical mixing exhibits exceptional passive power stability, reaching 0.8% RMS over a two-hour period. Furthermore, when the optical bandpass filter is controlled at the data wavelength of 1540 nm, we achieve up to 30 dBm of the overall mean output power with an optical conversion gain of 46 dB and an exceptionally high optical signal-to-noise ratio reaching 80 dB. Using orthogonal frequency division multiplexing (OFDM) signals, each data subcarrier is modulated using 128 quadratic amplitude modulation (128-QAM) at carrier frequencies f_k and simultaneously up-mixed to high aim frequencies $nf \pm f_k$ at the SOA-MZI output. Additionally, the resulting OFDM_128-QAM up-mixed signal is examined using the specifications for the error vector magnitudes (EVMs) and the electrical conversion gains (ECGs). The SOA-MZI mixing experiment can handle high frequencies up to 120 GHz. Positive ECGs are followed by a sharp reduction over the entire band of the aim frequencies. The highest frequency range achieved during the realistic investigation is shown at $2f + f_4 = 120$ GHz, where the EVM reaches 8% with a symbol rate of 15 GSymb/s. Furthermore, the concurrent OFDM_128-QAM up-mixed signal achieves an absolute maximum bit rate of 80.4 Gbit/s. The investigation into the simultaneous electro-optical mixing regime is finally supported by unmatched characterization improvements.

Keywords: electro-optical mixing; differential transformation; semiconductor optical amplifier Mach–Zehnder interferometer; quadrature amplitude modulation; orthogonal frequency division multiplexing

check for updates

Citation: Termos, H.; Mansour, A. SOA-MZI Differential Transformation Approach Applied on Simultaneous Electro-Optical Mixing. *Photonics* **2023**, *10*, 649. https://doi.org/10.3390/photonics10060649

Received: 5 March 2023
Revised: 15 May 2023
Accepted: 31 May 2023
Published: 3 June 2023

Copyright: © 2023 by the authors. Licensee MDPI, Basel, Switzerland. This article is an open access article distributed under the terms and conditions of the Creative Commons Attribution (CC BY) license (https://creativecommons.org/licenses/by/4.0/).

1. Introduction

It is crucial to conduct numerous studies to develop radio over fiber (RoF) and apply it in various applications such as radar fulfillment, wireless fidelity (WiFi), cellular networks, and millimeter-wave (MM-W) systems. Indeed, RoF can demonstrate a number of advantages, including an extremely high optical transformation data rate, minuscule weight, low expenditure, and a fairly high frequency range [1–5]. The effectiveness of any all-optical transmission implementation can be improved by all-optical mixing, which has many beneficial properties, including positive conversion efficiency at higher frequencies, high signal-to-noise ratio (SNR) values, and low quantities of error vector magnitude (EVM) amounts with peak bit rates dependent on the nonlinearity properties of various photonic mixing devices. Additionally, sampling optical mixers can be used to achieve logic gate operations, which are just as significant as optical mixing [6–16]. To achieve

frequency conversion, various technologies can be used, such as Mach–Zehnder modulators (MZMs) that achieve excellent performance [5,17], electro-absorption modulators (EAM) employing the cross-absorption modulation (XAM) [18,19] used for optical and electro-optical mixing processes, and many types of photodiodes (PDs) including uni-traveling carrier PDs (UTC-PDs) [20,21] and positive-intrinsic-negative PDs (PIN-PDs) [22] occupied for frequency mixing as a consequence of the contribution of their nonlinear photocurrent response and reverse voltage. More technologies are also achieved based on the semiconductor optical amplifier (SOA) predicated on nonlinear behaviors inclusive of the four-wave mixing (FWM) [23,24] and the cross-gain modulation (XGM) [25,26] impacts, and the SOA-Mach Zehnder interferometer (SOA-MZI) established on the cross-phase modulation (XPM) [27–31] leverage.

Due to their exceptional ability to display outstanding implementation, such as a high-frequency range, a high data transmission rate, and lofty conversion gains (CGs), SOA-MZIs have a remarkable apparatus for frequency transformation based on monocular, cascaded, and parallel arrangements [32–40]. The SOA-MZI can be incorporated with an optical pulse source (OPS) [41–43] that employs a mode-locked laser to create an optical pulse train with a very short duration determined in the picosecond (ps) of pulse width and a high repetition rate. This optical pulse train has a very low duration and is used as an optical switch. With a remarkable quality performance, SOA-MZIs can be used for mixing in the optical domain or in the electro-optical field [44–47]. Additionally, SOA-MZIs can be exploited for concurrent frequency switching using all-optical digital and analog signal processing algorithms that include bandpass sampling [48].

For every electro-optic arrangement, the recovery time of administered SOAs is fundamentally regarded as a restricting requirement. With notable improvements in the theories of spectrum conversion at a bit transmission rate up to 320 Gb/s with a high modulation bandwidth range, the improved gain dynamics of employed SOAs have significantly encouraged various design notions of data modulation at greater bit rates in addition to greater amendment bandwidth applications in all optical and electro-optical systems [49–51]. Along with contributing to the stimulated recombination time of carriers (τ_s), the differential carrier lifetime (τ_d) is a key factor in the SOA-MZI apparatus's dynamic properties. The resulting effective carrier lifetime (τ_e), which is obtained from τ_d and τ_s, primarily increases from dozens to hundreds of ps, depending on the applied SOAs [52]. Because of this, SOAs must be predisposed to a high bias current up to a maximum of 400 mA. The needed period of both SOA gains and phase calls for a quick recoup with the goal of preserving the exceptional mixing efficacy of electro-optic configurations. The initial photonic wavelength [42], which must be sufficiently near to enable swift recovery, plays a significant role in identifying this recovery time. Despite having a short runtime, the interferometer's coherent SOAs accurately consider a variety of expedited XPM and XGM nonlinear consequences as well as severe dynamics. Therefore, it will be useful to determine the influence of SOA parameters on the quality of mixed data communication through a straightforward examination of the coplanar elements of the electro-optic mixing transmitting mechanism. As a result of that, the SOA's carrier density is efficiently modulated by the large augmentation of the OPS repetition rate up to 39 GHz with a time interval reaching 1 ps among the optical pulse source (OPS) pulses [53], which reduces the variation of harmonic amplification with harmonic levels. As a consequence of this, at the SOA-MZI output, the electro-optical mixed signal carrying 128-QAM (Quadrature Amplitude Modulation) data is significantly authenticated and enhanced in terms of its properties.

A solo SOA has been up-to-now used in its nonlinear area to perform electro-optical switching [44,45]. A need for electro-optical mixing at higher frequencies obtained from the reflective SOA (RSOA) has thus far grown satisfactorily [44]. With a reasonable evaluation, the low frequency of a data signal carrying quadratic phase shift keying (QPSK) data has been up-mixed to a towering 15 GHz frequency with this method.

An electro-optical up-mixer originating from a SOA-MZI differential modulation arrangement was successfully implemented in our previous project [47]. By employing an

optical coupler (OC) at the optical port of the SOA-MZI, the OPS signal serves as an input sampling signal after passing through each SOA in the topmost and lower arms, while the intermediate-frequency (IF) signal is coupled to the electrical gate of each SOA utilizing the identical bias currents. The proposed electro-optical shifting regime exhibits compatible performance characteristics, including a frequency band up to 195.5 GHz, a data transition rate of 5 Gbit/s with low EVM amounts, and incredibly positive electrical conversion gains (ECGs). This is achieved using a well-known and widely deployed software program known as the VPI (Virtual Photonics Inc.) simulator [54].

In this ground-breaking study, we vigorously disseminate experimental outcomes of a simultaneous electro-optical mixing setup dependent on a SOA-MZI differential transformation approach that was entirely developed by utilizing the prior research shown in [47]. The interchange of incoming fields among electrical and optical input gates, which have various parameter attributes, represents the core difference between the new study dependent on the differential switching architecture and the prior one contingent on the differential modulation architecture [47]. A simultaneous signal with four channels is also used at the SOA-MZI optical interface. Finally, the photonic filter is controlled at the optical frequency of the channels, where it is tuned at the wavelength of the control signal [47]. As a result, four data signals are simultaneously inserted into the optical port of the SOA-MZI, and two OPS signals with the same structure and exceptional features are introduced to the electrical gate of SOAs. Furthermore, the OPS signal's position at every SOA's electrical entrance is capable of raising the replica power of the concurrent up-mixed signal. This replica power is influenced by the OPS signal's harmonics, which are crucial for controlling the electro-optical system and achieving simultaneous mixing. This striking improvement results from the OPS signal's unique characteristics, which include a high repetition rate of 58.5 GHz and a very brief pulse width of 1 ps. By utilizing these important features, it is possible to create a simultaneous up-mixed signal that has copies following the first two OPS harmonics and stunning experimental results. Therefore, the realistic electro-optical mixing system, which originated from four simultaneous data signals, is newly assessed in the optical field and also in the electrical branch and has attractive attributes, particularly power stability, a high optical signal-to-noise ratio (OSNR), a frequency switching range up to 120 GHz, approaching substantially conversion gains (CGs), and the demodulation of the OFDM (Orthogonal Frequency Division Multiplexing) up-mixed signal, where its data subcarriers are modulated using 128-QAM (Quadrature Amplitude Modulation) data at a bit rate of 80.4 Gbit/s in the course of a significant parameter known as EVM.

2. SOA-MZI Differential Transformation Principle of the Simultaneous Electro-Optical Mixing

The Center for Integrated Photonics (CIP) organization [41] produced the SOA-MZI configuration used in our experimental work and shown in Figure 1. Incoming electro-optical mixing from a SOA-MZI differential transformation pattern is further described in this illustration. This new assumption has evolved as a result of our earlier research [47].

At the electrical gates of the top and bottom SOAs in such a system, the control signal is implanted at a repetition rate of f. Similar to this, data signals at the frequencies f_k are simultaneously pumped into each SOA-MZI appendage via an optical coupler (OC). Thus, the carrier density in conjunction with the refractive index of each SOA is cogged by the control signal at the electrical gate through a bias current in every arm, and posteriorly, the control signal modulates each data signal in joint arms. At the optical output of the SOA-MZI, the up-mixed signal is established at desired frequencies $nf \pm f_k$ after sampling between the control and data signals. The differential transformation based on the electro-optical system can unconventionally realize simultaneous mixing for k channels of data signals with outstanding quality. Because the up-mixed signal is produced after filtering at one of the wavelengths of the data signals, its replica power decreases with frequency. As a result, the control signal is transferred at a wavelength of the data signals, which decreases the harmonic power of the control signal as well as the replicas' power at $nf \pm f_k$.

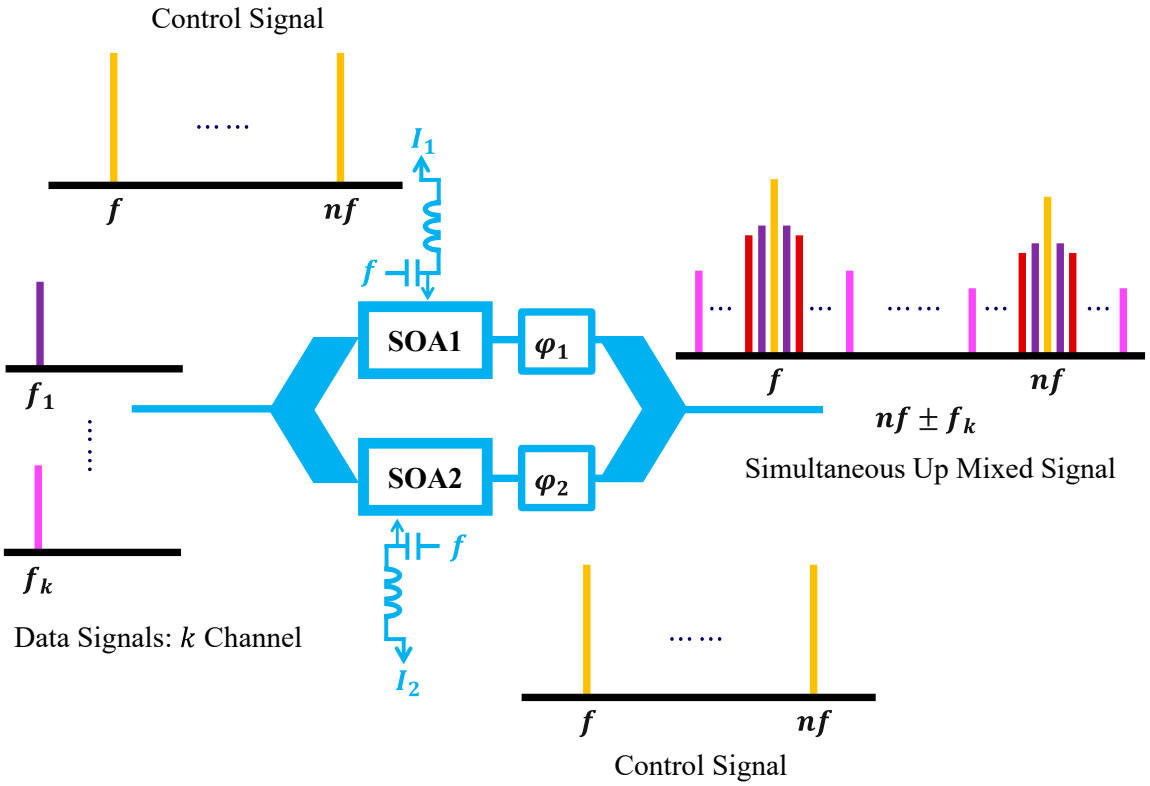


Figure 1. Simultaneous electro-optical mixing operation originated from a SOA-MZI differential transformation regime.

The only solution to augment the harmonics along with the replicas is to apply the differential modulation regime [53], where the data signals are converted at the wavelength of the control signal at the SOA-MZI output. It is vital to mention that in the differential modulation architecture, the data signals modulate the sampling pulse train known as the OPS signal. In particular, at the SOA-MZI optical gate, the 3 dB optical coupler now splits the OPS signal into two similar duplicates. The top and bottom duplicates of the OPS signal are, in this instance, phase-shifted by the data transmission signals. As a result, the amplified OPS signal's parts that occur at the uppermost and lowermost outturns continuously vary, which are a modulation of the OPS signals by the data signals.

3. Performance of the Simultaneous Electro-Optical Mixing System for Up Mixing Using a SOA-MZI Transformation Configuration

3.1. Experimental Setup

The experimental setup of simultaneous electro-optical sampling derived from a SOA-MZI differential transformation principle is presented in Figure 2. The SOAs were driven by the same bias current, i.e., $I_1 = I_2 = 400$ mA.

The optical pulse sources (OPSs) used in this realistic setup comprise a mode-locked fiber laser created by Pritel Inc. (Naperville, IL, USA) [41–43]. In addition to the OPSs construction, OPS signals have the key operating point that ameliorates the simultaneous electro-optical mixing system. These measurable factors are a wavelength of $\lambda = 1550$ nm, a pulse width duration of 1 ps, a repetition rate of $f = 58.5$ GHz, a peak optical power of -1 dBm, and a purposeful duty cycle of 5.85%, which are applied to the OPS signals at the electrical ports of the topmost and inferior SOAs. The optical pulsed signal is converted to an electrical one by utilizing a photodiode (PD) and then electrically amplified by a low noise amplifier (LNA) before intercalating into the SOAs electrical gate. The electrical OPS signal shows the first harmonic at a frequency of $H_1 = f$ and the second one at $H_2 = 2f$, as presented in Figure 3, where their amplitudes stay low with the frequency. The difference

between both harmonics is 3 dB. Depending on its repetition rate, the OPS always generates a high noise level at the higher harmonic frequency. This noise level will be completely reduced at the SOA-MZI exit by employing an optical bandpass filter (OBPF).

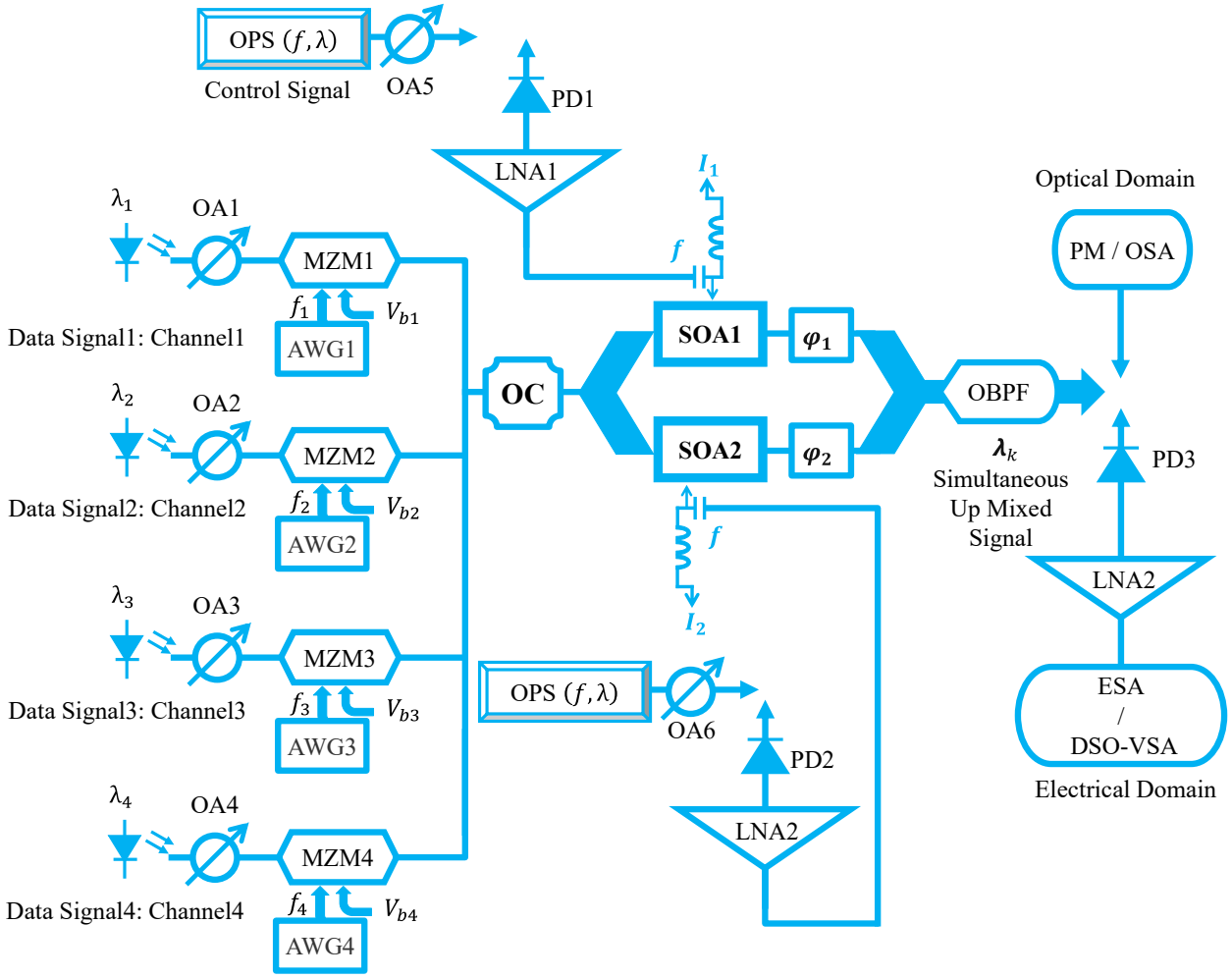


Figure 2. Experimental setup of the simultaneous electro-optical mixing using a SOA-MZI differential transformation principle. ESA: Electrical Spectrum Analyzer, OSA: Optical Spectrum Analyzer, OA: Optical Attenuator, OBPF: Optical Band Pass Filter, AWG: Arbitrary Waveform Generator, LNA: Low-Noise Amplifier, PD: Photodiode, PM: Power Meter, DSO: Digital Sampling Oscilloscope, VSA: Vector Signal Analyzer, φ: phase shifter, SOA: Semiconductor Optical Amplifier, SOA-MZI: SOA-Mach Zehnder Interferometer, V_b: bias voltage, OPS: Optical Pulse Source.

On the other hand, k data signals at a range of intermediate frequencies (IFs) were employed at the optical gate of the SOA-MZI. We chose $k = 4$ in this investigative study in order to avoid the complexity of the requested optical communication system, while we could concurrently select higher k channels up to twenty depending upon their data frequencies. The four data signals had specifications, such as wavelengths $\lambda_1 = 1540$ nm, $\lambda_2 = 1542$ nm, $\lambda_3 = 1545$ nm, and $\lambda_4 = 1548$ nm and optical average powers of -16, -14, -12, and -10 dBm, respectively. Following photodetection by a PD and an electrical power augmentation by a LNA, the electrical powers of the data signals were -40.1, -35.2, -30.1, and -25.1 dBm, respectively. Additionally, the data signals were intensity modulated by OFDM (Orthogonal Frequency Division Multiplexing) technology at carrier frequencies of $f_1 = 0.75$ GHz, $f_2 = 1.5$ GHz, $f_3 = 2.25$ GHz, and $f_4 = 3$ GHz, appropriately, where its data subcarriers totaled 128-QAM (Quadrature Amplitude Modulation) format modulations.

The OFDM_128-QAM data originated from arbitrary waveform generators (AWGs) at the electrical gate of the optical Mach-Zehnder modulators (MZMs).

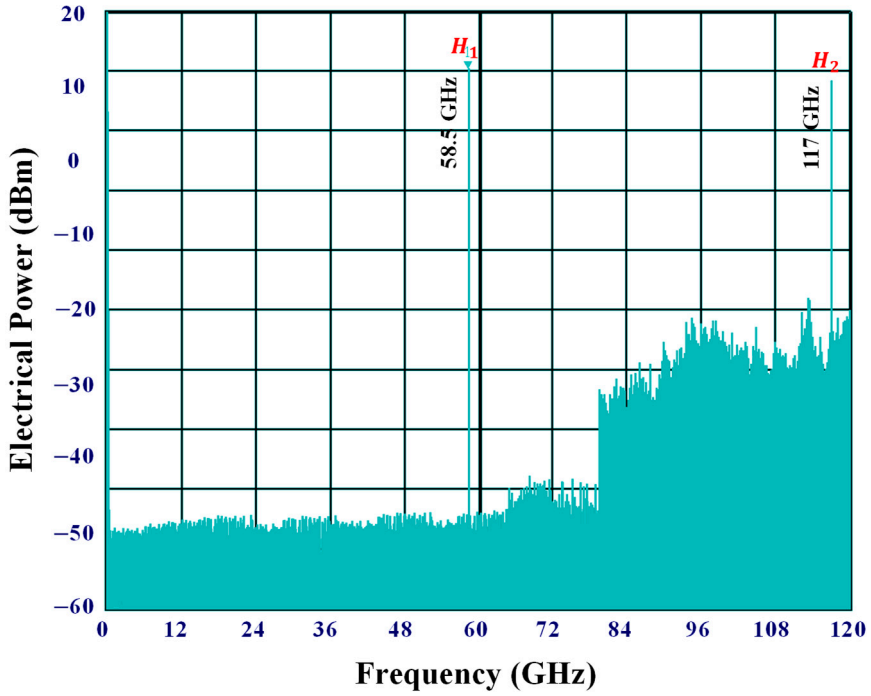


Figure 3. OPS electrical spectrum at the electrical stage of each SOA at frequencies $H_n = nf$.

The optical band pass filter (OBPF) was configured at 1540 nm to analyze the contemporaneous electro-optical mixing system in the electrical domain, while it was controlled at a variety of wavelengths on the way out of the SOA-MZI for investigating the system in the optical sector. To reduce the impact of the amplified spontaneous emission (ASE) power coming from the SOAs, the OBPF had a bandwidth of 0.56 nm of full width at half maximum (FWHM). The concurrent electro-optical transmission system had excellent distinctive characteristics at low input power instructions; hence, this 1540 nm wavelength was chosen. After that, a PD enabled the simultaneous up-mixed signal. All of the PDs used in this experiment had the following specifications: a 300 GHz bandwidth, 0.85 A/W sensitivity, and minimal shot noise. The uni-traveling carrier photodiode (UTC-PD), which is only applied for photo-detection, was frequently employed at frequencies over 120 GHz in this article. Considering its remarkable capabilities in terms of substantial generated power as well as broad bandwidth, where -3 dB bandwidths are as high as 310 GHz, this kind of photodiode was employed [55,56] in our experimental setup. Thereupon, the electrical mixed signal was magnified by a 33 dB-gain LNA and propounded on an electrical spectrum analyzer (ESA) to produce the desired spectrum of the simultaneous up-mixed signal. On the other hand, in order to demodulate the simultaneous 128-QAM up-mixed signal that carries 128-QAM data and evaluate the electro-optical shifting system by obtaining EVMs (Error Vector Magnitudes) or bit error rate (BER) hallmarks, we applied this signal on digital sampling oscilloscope (DSO) hardware and vector signal analyzer (VSA) software over a series of symbol rates.

The SOA-MZI behavior was studied for each data signal at distinct parameters, as shown in Figure 4. The extinction ratio (ER) is a commensurable factor to evaluate the SOA-MZI performance attributes. The ER is elaborated as a difference between the largest and lowest optical conversion powers at the SOA-MZI outlet. The advantageous operating point was employed to upgrade the ER values and consequently to ameliorate the simultaneous up-mixed signal at the SOA-MZI output with outstanding quality and efficiency of the electro-optical mixing system depending upon the differential SOA-MZI transformation principle. Each data signal, along with its specifications, was individually injected into the

optical port of the SOA-MZI input. Moreover, the input optical power of the control signal was changed from −40 to 5 dBm at a wavelength of 1550 nm. The maximum ER of 30 dB was achieved for the first data signal, when the input control power was −1 dBm. This ER downgraded to 24 dB for the fourth data signal at −1 dBm.

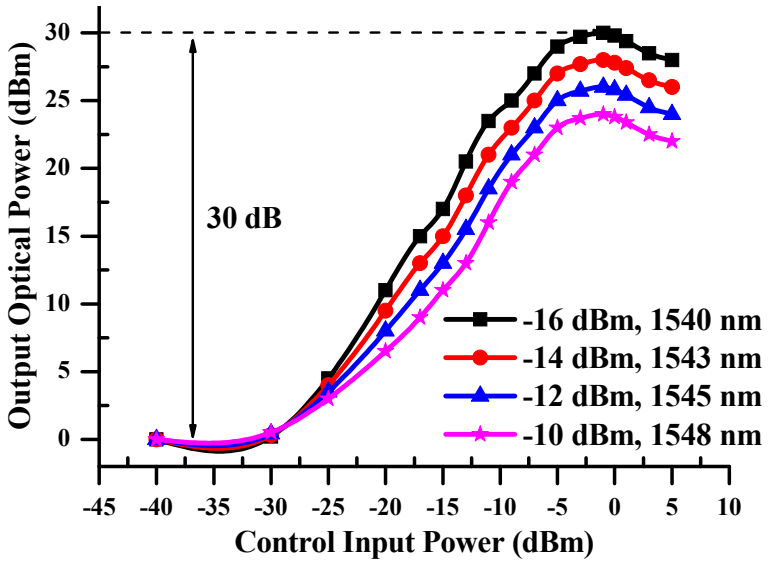


Figure 4. SOA-MZI static behaviors for each data signal features.

It is vital to recall that the main originality of this paper is the application of four channels, which had different attributes including wavelengths and optical average powers, at the SOA-MZI input optical gate. Moreover, the efficiency and quality of the electro-optical simultaneous up mixing system were studied when the OPBF was regulated at each wavelength of the four channels. If they had the same wavelengths, it would have been difficult to characterize the experimental results, especially the replicas of the four channels at the SOA-MZI output, when the OBPF would be tuned at the identical wavelength of the four channels. Studying the operating point of the simultaneous electro-optical system is very important in order to achieve vital outcomes. Figure 4 displays the static characteristics of the employed SOA-MZI for different wavelengths before achieving the simultaneous mixing function. With this figure, we are able to identify that the best characteristic was at 1540 nm with a higher extinction ratio. Hence, the simultaneous signal at the SOA-MZI output will have higher features, including OCG, at this wavelength.

3.2. Optical Characteristic Attributes

(a) Output Power Characterizations

The output optical power values of the simultaneous up-mixed signal relied on the electro-optical sampling system applying a photonic SOA-MZI differential transformation method, which was measured at its exit by using a power meter (PM) apparatus, as presented in Table 1. When the OBPF was individually changed at one of the data signal wavelengths, the output optical power was acquired at each value. In that scenario, we achieved four optical output power amounts, with the largest one being 30 dBm at 1540 nm, as already shown in Figure 4. This wavelength corresponded to the first data stream, which had an input optical power of −16 dBm. The primary data signal had a larger ER of 30 dB, which essentially resulted in a higher output converted power of 30 dBm, as previously shown in Figure 4.

Table 1. Output power ranges of the simultaneous up-mixed signal.

Input Data Signals (Powers (dBm) and Wavelengths (nm))	OBPF Wavelength (nm)	Output Optical Power of the Simultaneous Up Mixed Signal (dBm)
Data Signal 1: −16, 1540	1540	30
Data Signal 2: −14, 1543		
Data Signal 3: −12, 1545		
Data Signal 4: −10, 1548		
Data Signal 1: −16, 1540	1543	25
Data Signal 2: −14, 1543		
Data Signal 3: −12, 1545		
Data Signal 4: −10, 1548		
Data Signal 1: −16, 1540	1545	20
Data Signal 2: −14, 1543		
Data Signal 3: −12, 1545		
Data Signal 4: −10, 1548		
Data Signal 1: −16, 1540	1548	15
Data Signal 2: −14, 1543		
Data Signal 3: −12, 1545		
Data Signal 4: −10, 1548		

(b) Optical Conversion Gain

In optical scope characterizations, the optical conversion gain (OCG) of the simultaneous up-mixed signal is considered to be an excellent parameter for assessing the concurrent electro-optical mixing system using the SOA-MZI transformation mechanism and is exhibited in Figure 5. It is expounded as an inequality determined in dB between the output power of the simultaneous up-mixed signal at the SOA-MZI output and the optical data powers of the four IF signals at the SOA-MZI input. Each time the OBPF was altered at one of wavelengths of the data signals, we obtained a distinct range of the OCG values.

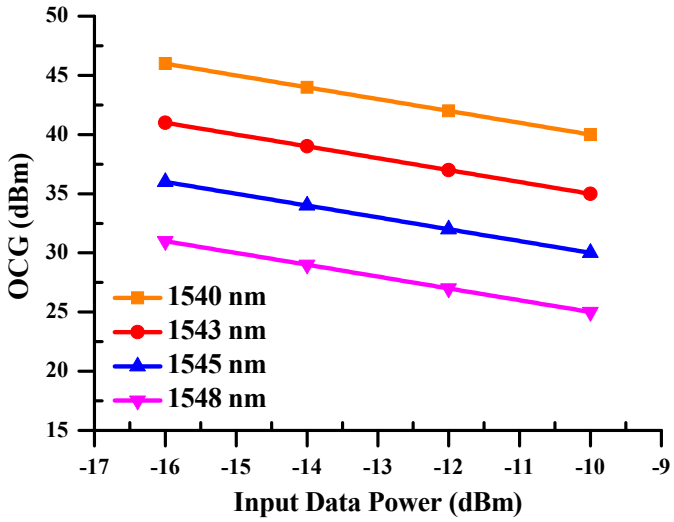


Figure 5. OCG of the simultaneous up-mixed signal when the OBPF is separately tuned at the wavelengths of the data signals.

The OCG is shown in Figure 5 as a function of the input data power for various wave lengths. Over the full range of incoming data powers, the maximum number of OCGs was found at 1540 nm. This amply demonstrates that SOA-MZI is capable of achieving an excellent sampling operation at 1540 nm with a low incoming power consumption. As a result, the following experimental observations for mixing examinations in the optical and electrical fields mostly used the OBPF wavelength regulated at 1540 nm. In that case, all the data signals were switched at the SOA-MZI outturn at 1540 nm as well as the sampling control signal in order to produce the desired simultaneous up-mixed signal.

(c) Output Power Stabilization

The ability of a powerful and efficient system to maintain an operational balance is proven by the power stability of that system. A long-term power stability, 30 ± 0.5 dBm, as shown in Figure 6, was another characteristic of the simultaneous up-mixed signal at the SOA-MZI output, which was derived from the electro-optical mixing regime employing its differential transformation approach. In order to complete all realistic measurements of the electro-optical mixing system, the output optical power was written down to overture beneficial passive stability of about 0.8% RMS (Root Mean Square) for the concurrent up-mixed signal over a duration of two hours. This value indicated a very slight variance in the output power, which was a great characteristic for evaluating our system. It is important to emphasize once more that the contemporaneous up-mixed signal was optically filtered at the SOA-MZI exit at the main wavelength of 1540 nm.

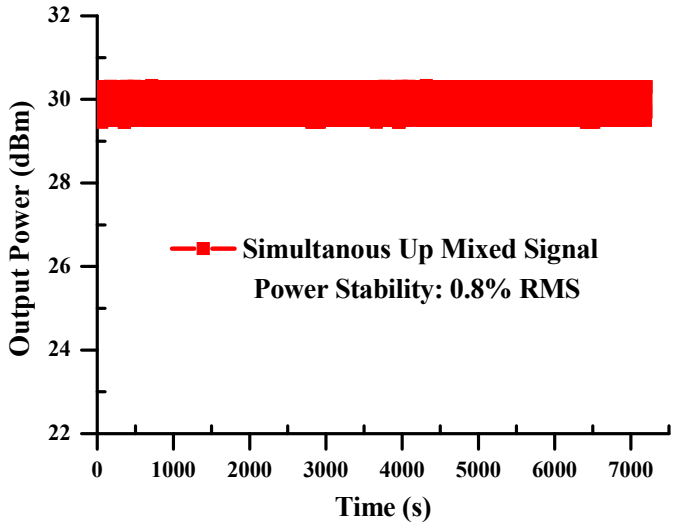


Figure 6. Power stability of the simultaneous up-mixed signal obtained at 1540 nm at the SOA-MZI output.

(d) Signal to Noise Ratio

The optical signal-to-noise ratio (OSNR), which is used in many industries including wireless communications and photonic telecommunication systems, is also an important consideration for evaluating our simultaneous electro-optical mixing regime [57]. The OSNR characterization is defined as the disparity, measured in dB, between the signal and noise powers at the photonic SOA-MZI mixer's input and output. Thus, the SOA-MZI output successfully achieved the OSNR value of the concurrent up-mixed signal at 1540 nm. It had an optical output power of 30 dBm and a noise power of 52 dBm. This resulted in an outstanding output OSNR at 1540 nm of 82 dB. When the OBPF was modified at other wavelengths, as we previously did for the output power scaling, the output OSNR was also tested to confirm the peak value of the simultaneous up-mixed signal at 1540 nm.

Figure 7 illustrates the input OSNR for each data signal as well as the output OSNR values in comparison to the data wavelength. As seen in Figure 7, we could demonstrate that at 1540 nm, the input and output OSNR were at their greatest values. Additionally,

due to the significant noise produced at the SOA-MZI output, the output OSNR degraded by 20 dB at 1545 nm, while the input OSNR at the SOA-MZI input only deviated by 4 dB. It should be noted that the SOAs amplified spontaneous emission (ASE), which subjoined supplemental noise at the SOA-MZI output after optical amplification and mixing processes, which impacted significantly the optical simultaneous up-mixed signal. In addition, the transmutation mechanism from optical to electrical fields caused the PD to produce shot and thermal noises at the receiver [58].

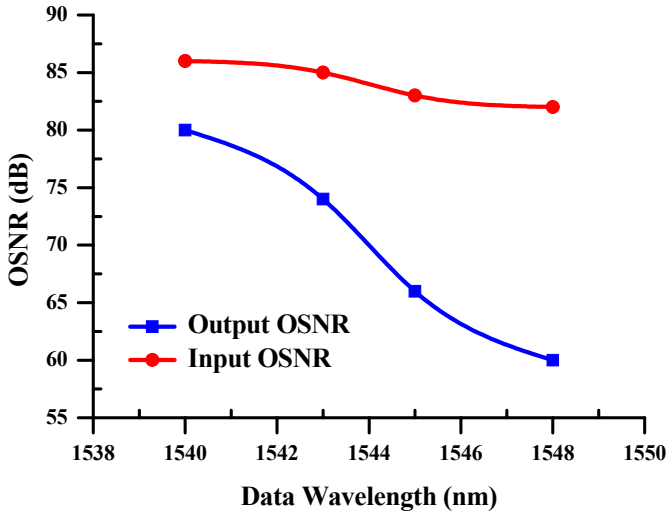


Figure 7. Input and output OSNR values of the simultaneous electro-optical mixing system as a function of the data wavelengths.

(e) Noise Figure

Figure 8 illustrates the noise figure (NF), which is another important parameter for characterizing the simultaneous electro-optical mixing regime reliant on the SOA-MZI differential transformation approach [59,60].

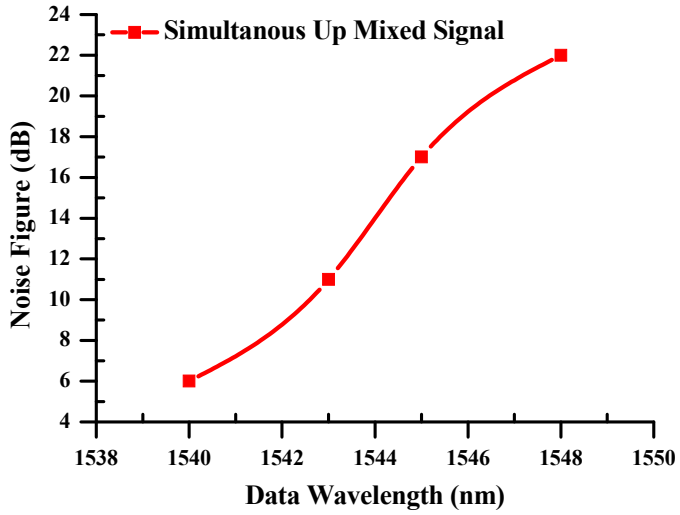


Figure 8. NF of the simultaneous up-mixed signal at the SOA-MZI output for several data wavelengths.

The NF is defined precisely as the variation between both the input and the output OSNR, measured in decibels (dB). The data wavelength and the input data power of the IF signal [61–64] have a significant impact on the NF of the concurrent up-mixed signal, which is a key indicator of the effectiveness of our electro-optical switching system. The measured NFs are shown in Figure 8 for a variety of wavelengths. Because the OBPF was independently adjusted at the wavelengths of the data signals, the output OSNR had four

values. In those conditions, the simultaneous up-mixed signal had four different NF values that were in sharp contrast with one another. Peak levels of 6 dB at 1540 nm highlighted the coterminous electro-optical mixing system's remarkable performance.

(f) Optical Spectrum

When the OBPF was adjusted at 1540 nm, one of the optical spectra of the concomitant up-mixed signal at the SOA-MZI egress that was determined by employing an optical spectrum analyzer (OSA) is shown in Figure 9 in order to validate the experimental results indicated above. At 1540 nm, it had an average output power of 30 dBm, and the OSNR was 82 dB.

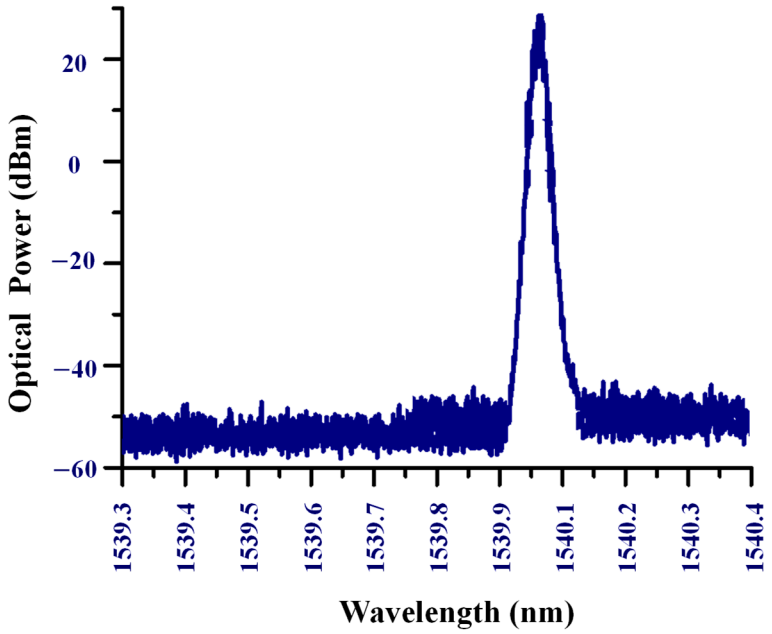


Figure 9. Optical spectrum of the simultaneous up-mixed signal at the SOA-MZI output at 1540 nm.

3.3. Electrical Characteristic Attributes

(a) Electrical Spectrum

Implementing the SOA-MZI differential transformation methodology requires an exceedingly accurate assessment of the concurrent electro-optical mixing procedure of the four data signals throughout an electrical spectrum. Figure 10 adequately validates the simultaneous up-mixed signal at aim frequencies $nf \pm f_k$ originating from the four data signals at f_k, which were also magnified at the SOA-MZI output. Moreover, there was an understandable retraction of 7 dB between the first harmonic power at $f = 58.5$ GHz and the second one at $2f = 117$ GHz of the sampling OPS signal with the frequency in this spectrum. As a result, the OPS harmonics, where electrical strengths decreased with the aim frequency, were tracked by replicas of the contemporaneous up-mixed signal.

It is important to note that the OPS performance, particularly its repetition rate of 58.5 GHz and the pulse width duration of 1 ps, was the primary factor that resulted in the experimental outcomes of the concurrent electro-optical system. Since we already attained the identical optical characterizations at 1540 nm as before, the best electrical spectrum was ultimately produced when the OBPF was adjusted at this wavelength, which is that of the initial data signal. Therefore, since we would obtain the same spectrum design with reduced electrical powers of the OPS harmonics as well as the replicas, there was no requirement for getting an electrical spectrum of the simultaneous up-mixed signal at each wavelength. As a result, the simultaneous electro-optical mixing system was only evaluated in the electrical field when OBPF was adjusted at 1540 nm. It is crucial to recall that the PD, LNA, and OBPF losses were all taken into consideration through all primary measures and arithmetic rules.

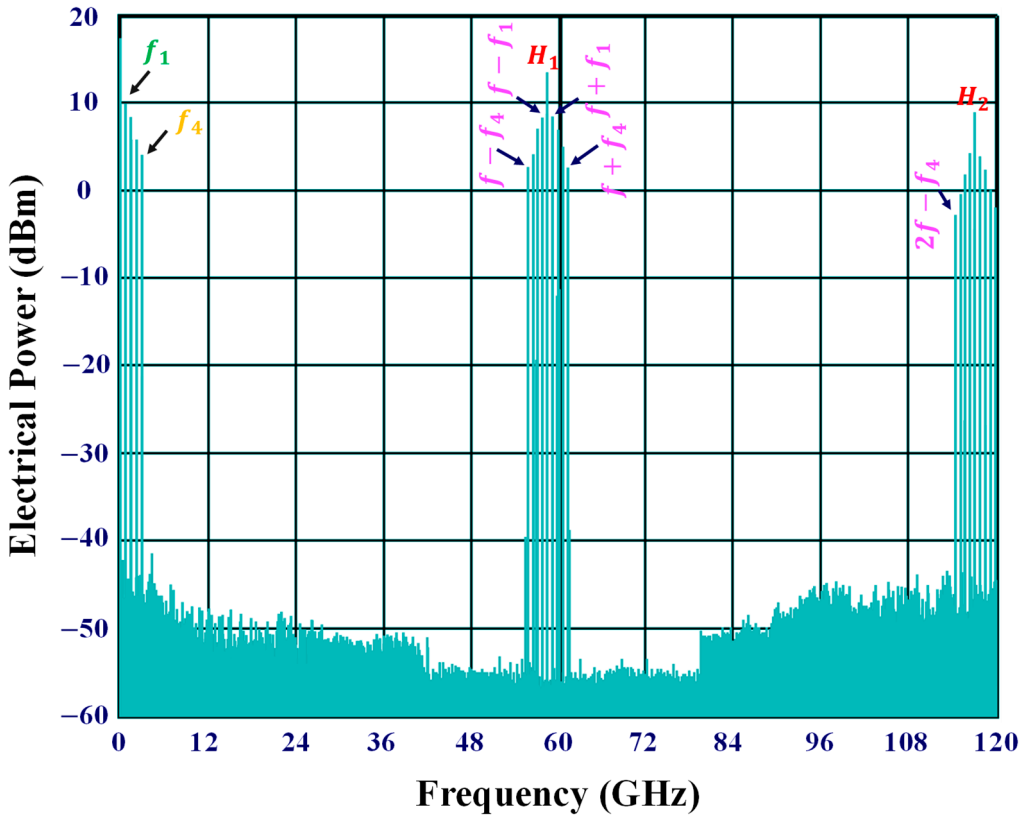


Figure 10. Electrical spectrum of the simultaneous up-mixed signal at the SOA-MZI output at aim frequencies $nf \pm f_k$ derived from the four data signals at f_k.

(b) Electrical Conversion Gain

The most popular method for analyzing the characteristic performance of the concurrent electro-optical differential transformation system using the SOA-MZI as an electro-optical switch is electrical conversion gain (ECG) calculations, as provided in Table 2. The ECG is best contemplated in dB and is classically recognized as the difference in electrical powers obtained in dBm between replicas of the simultaneous up-mixed signal at aim frequencies $nf + f_k$ at the SOA-MZI outturn and the data signals at carrier frequencies f_k at the SOA-MZI input. Additionally, the desired sidebands of the replicas were chosen to be at the right of the harmonics for ECG calculations.

Table 2. ECGs of the simultaneous electro-optical mixing system at $nf + f_k$ using the differential transformation mechanism.

	Aim Frequency (GHz)	Replicas Power (dBm)	Data Power (dBm)	ECG (dB)
Simultaneous Up-Mixed Signal at $f + f_k$	59.25	8	−40	48
	60	7	−35	42
	60.75	5.5	−30	35.5
	61.5	3.5	−25	28.5
Simultaneous Up-Mixed Signal at $2f + f_k$	117.75	4	−40	44
	118.5	3	−35	38
	119.25	0	−30	30
	120	−3	−25	22

As shown in Table 2, the simultaneous electro-optical mixing topology had a typical recommended value of peak ECG of 48 dB at $f + f_1$, which was related to the first harmonic of the OPS signal $H_1 = f$ as well as the first data signal. The ECGs, which significantly decreased with the aim frequency, were much improved by this concurrent telecommunication system.

At $f + f_k$, the ECG difference of the simultaneous up-mixed signal between the replica at $f + f_1 = 59.25$ GHz related to the first data signal and the replica at $f + f_4 = 61.5$ GHz linked to the fourth one was 19.5 dB. This difference at $2f + f_k$ associated with the second harmonic $H_2 = 2f$ was 22 dB. Furthermore, the maximum frequency range of this simultaneous system was 120 GHz, which corresponds to the aim frequency of the fourth replicas at $2f + f_4$. The recently developed simultaneous electro-optical sampling system therefore produced high positive ECGs, which encouraged the system's high efficiency. The OPS distinguishing characteristics and the modest requirements for the input data powers were responsible for the performance growth of this modernistic arrangement. Utilizing simultaneous electro-optical mixing operations could effectively overpower the corollary of the parasitic components and greatly enhance the ECG.

(c) Isolation

As shown in Figures 11 and 12, isolation obtained in dB at the SOA-MZI output can also be utilized to assess the effectiveness of the contemporaneous electro-optical mixing system. The isolation values are simply defined as the difference in electrical power measured in dBm between the OPS signal (local oscillator, or LO) and the simultaneous up-mixed signal (RF), known as LO-RF isolation, or between the data signal (intermediate frequency, or IF), and the RF signal, known as IF–RF isolation.

LO-RF and IF-RF isolations were computed at the SOA-MZI output, as displayed in Figure 11, at aim frequencies $f + f_k$ related to the first harmonic $H_1 = f$ of the OPS signal and in Figure 12 at $2f + f_k$ linked to the second harmonic $H_2 = 2f$. The LO-RF isolation, between the OPS signal at frequencies $H_n = nf$ and the simultaneous up-mixed signal at $nf + f_k$, augmented with the aim frequency connected to each data signal as well as both harmonics in each individual figure. Because of the degradation of replicas of the simultaneous up-mixed signal at $2f + f_k$ correlating to H_2 as well as the second harmonic power of the OPS signal, the LO-RF isolation became profoundly larger, as given in Figure 12.

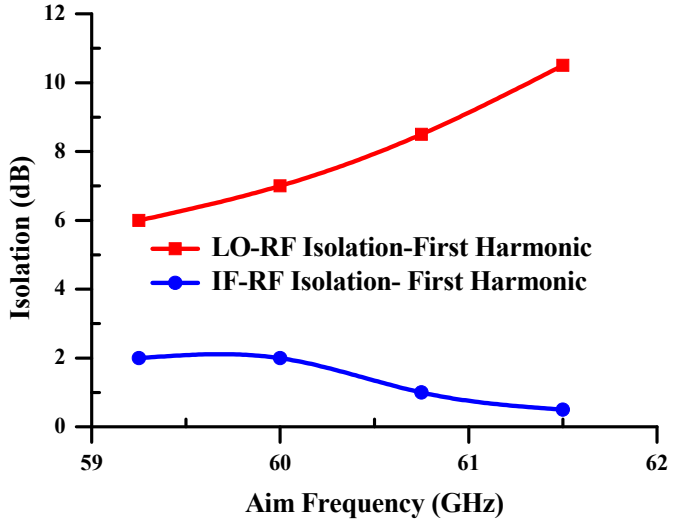


Figure 11. LO-RF and IF-RF isolations at the SOA-MZI output at the aim frequencies $f + f_k$ related to the first harmonic of the OPS signal. LO: Local Oscillator, IF: Intermediate Frequency, and RF Radio Frequency.

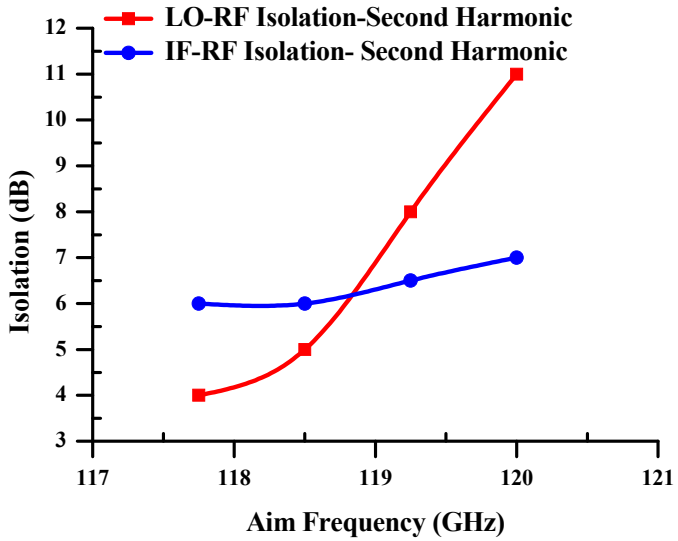


Figure 12. LO-RF and IF-RF isolations at the SOA-MZI output at $2f + f_k$ related to the second harmonic.

On the other hand, strong LO-RF isolation is crucial because it significantly reduces the self-mixing situation, which is a harmful circumstance brought on by mixing between the parasitic components and the concurrent RF signal [65]. Additionally, the self-mixing phenomenon causes a DC offset that degrades the performance of the simultaneous optical transmission system.

The IF-RF isolation between the data signal at f_k and the simultaneous up-mixed signal at $nf + f_k$, decreased slightly from 2 dB at 59.25 GHz related to the first data signal and to 0.5 dB at 61.5 GHz associated with the fourth data signal, as shown in Figure 11, interconnected to H_1. As seen in Figure 12, corresponding to H_2, the IF-RF isolation increased somewhat with the aim frequency ranging from 117.75 to 120 GHz. This was due to the declination of the replicas of the concurrent up-mixed signal originating from the data signal related to H_2, while the amplified power of the data signals at the SOA-MZI output illustrated in Figure 10 retained the same value when calculating the IF-RF isolations in both cases.

(d) Phase Noise

Phase noise (PN) characteristics displayed in Figure 13 are extremely imperative in many applications, especially in electro-optical communication systems. PN identifies variations in short time stability in the frequency field. The PN parameter is measured in dBc/Hz and is always negative. Moreover, it is assessed over a range of offset frequencies from 10 Hz to 1 MHz. The PN that is realized by using an electrical spectrum analyzer (ESA), which is a general-purpose instrument and flexible, can be derived as a difference between replica powers obtained in dBm of the simultaneous up-mixed signal and the noise signal power in a 1 HZ bandwidth at a particular offset frequency from the replica [66–68].

In our measurements, we took many spot noises that were PN at a certain offset frequency in order to plot PN as a function of the frequency offset for each replica related to the first and second harmonics of the OPS signal. As seen in Figure 13, the PN of the fourth replica of the simultaneous up-mixed signal was measured at the aim frequency of $f + f_4 = 61.5$ GHz related to the first harmonic H_1 and at $2f + f_4 = 120$ GHz linked to the second harmonic H_2 at the SOA-MZI output. As shown in Figure 13, between 10 Hz and 1 MHz, the PN of the replica associated with H_2 was degraded by a mean value of 10 dB compared to the one of the replicas related to H_1.

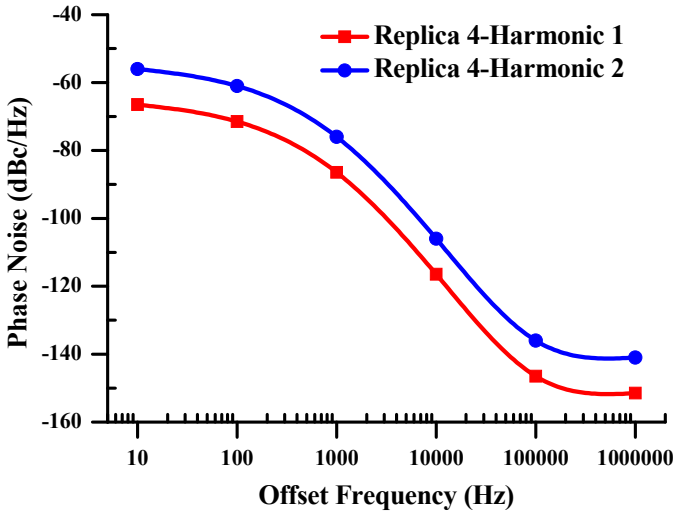


Figure 13. Characteristics of the simultaneous up-mixed signal through PN for the fourth replica of $f + f_4 = 61.5$ GHz related to the first harmonic and at $2f + f_4 = 120$ GHz related to the second harmonic.

(e) Error Vector Magnitude

OFDM (Orthogonal Frequency Division Multiplexing) modulation was carried with the data signals in order to enable contemporaneous electro-optical mixing based on the SOA-MZI differential transformation approach. Hence, the simultaneous OFDM up-mixed signal at the SOA-MZI output was instituted from the conversion of four data signals at the SOA-MZI input. This concomitant up-mixed signal was studied at a complete series of symbol rates spreading from 1 to 15 GSymb/s for the replica at the highest aim frequency of $f + f_4 = 61.5$ GHz related to H_1 and $2f + f_4 = 120$ GHz associated with H_2.

The OFDM data were originated by an arbitrate waveform generator (AWG) at a variety of carrier frequencies at the electrical gate of the optical MZM, where its output signal after modulation was introduced at the optical port of the SOA-MZI input. Each carrier frequency related to a particular data signal, as mentioned before in the experimental setup, consisted of a number of OFDM subcarriers, which were split into data subcarriers carrying 128-QAM (Quadratic Amplitude Modulation), pilot subcarriers, guard lower and upper subcarriers, and a concentrated null subcarrier [34,41,69]. In order to calculate the bit rate of the coterminous OFDM up-mixed signal, the symbol rate, the subcarrier number, the data subcarriers, and the number of bits must be identified. In this study, the number of bits was chosen to be 7, corresponding to 128-QAM, the subcarrier number of 128 was applied to the OFDM data for every data signal with 98 data subcarriers, and we used a fixed cyclic prefix (CP) of 25%. Equation (1) illustrates how the CP and SR are connected to the bandwidth (BW) of the OFDM signal [41]. The BW corresponds to 18.75 GHz when the SR is 15 GSymb/s.

$$BW = SR * (1 + CP) \quad (1)$$

The quality performance of the coeval electro-optical mixing system is considerably improved through the error vector magnitude (EVM) [57,70,71] parameters seen in Figure 14, which are attained by a vector signal analyzer (VSA) application after digitalizing by a digital sampling oscilloscope (DSO). Additionally, the deliberated EVM values are theorized to take measurements of the precision and reliability of OFDM_128-QAM modulation [72], contingent on the SOA-MZI differential transformation mechanism.

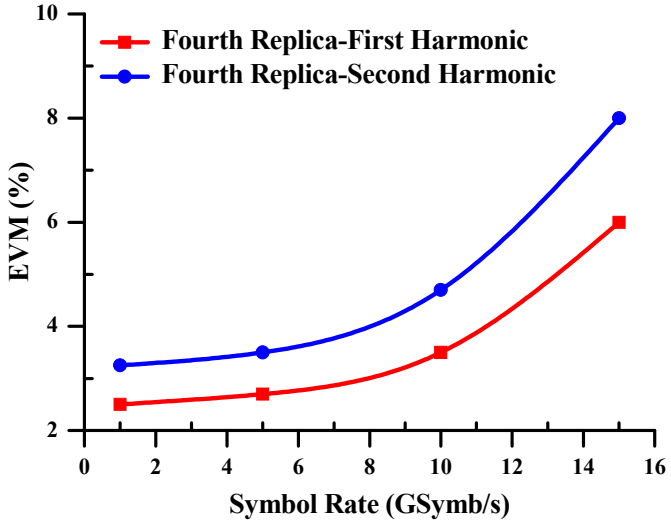


Figure 14. EVM measurements of the simultaneous OFDM_128-QAM up-mixed signal for the fourth replica related to first and second harmonics.

As seen in Figure 14, the EVM of the simultaneous OFDM_128-QAM up-mixed signal aggrandized with the symbol rate for the fourth replica at $f + f_4 = 61.5$ GHz as well as at $2f + f_4 = 120$ GHz. The EVM value reached 8% at 120 GHz; while it was 6% at 61.5 GHz at 15 GSymb/s. Furthermore, the maximum bit rate of the simultaneous OFDM_128-QAM up-mixed signal was calculated for the fourth replica, and its value was 80.4 Gbit/s. The investigation and amelioration of the simultaneous up-mixed signal dependent on the SOA-MZI used as an electro-optical switch mainly come from the OPS signal harmonics, where its replicas follow these harmonics, and also from the interestingly new electro-optical differential transformation regime.

4. Conclusions

We enumerate a novel design of a simultaneous electro-optical mixing system dependent on a SOA-MZI differential transformation approach. The performance validation of this electro-optical regime is exceptionally recognized in the optical and electrical fields. Many vital experimental results generated at the SOA-MZI output are optically and electrically achieved through this study, such as optical conversion gain (OCG), optical signal to noise ratio (OSNR), noise figure (NF), electrical conversion gain (ECG), phase noise (PN), and error vector magnitudes (EVMs). In terms of the optical performance features, the simultaneous up-mixed signal divulges excellent passive power stability of 0.8% RMS over 2 h. Moreover, we have achieved an OCG as high as 46 dB at the SOA-MZI output, and the output OSNR of 80 dB is examined carefully to be outstanding in the simultaneous electro-optical configuration when the OBPF is tuned at 1540 nm. In terms of electrical performance attributes, the efficiency as well as the quality of the simultaneous electro-optical mixing system were predominantly assessed by the ECG and EVM parameters. Furthermore, high positive ECGs are accomplished for all replicas over a comprehensive range of aim frequencies. The maximum ECG of 48 dB of the first replica is obtained at $f + f_1 = 59.25$ GHz, related to the first harmonic of the OPS signal, while it is 44 dB at $2f + f_1 = 117.75$ GHz, linked to the second harmonic. The simultaneous OFDM_128-QAM electro-optical mixing manifests remarkable EVM values up to 8% at 15 GSymb/s for the fourth replica associated with the second harmonic. The maximum frequency range of this simultaneous electro-optical mixing arrangement is 120 GHz, and the uttermost bit rate is 80.4 Gbit/s. The high repetition rate of 58.5 GHz and the low pulse width duration of 1 ps for the OPS signal with the SOAs gain greatly upgrade the quality performance of the simultaneous electro-optical SOA-MZI switch, particularly by improving the output replica power. Finally, the simultaneous mixing hinged on the electro-optical SOA-MZI differential transformation principle

is substantiated with preeminent performance enhancement. Thence, this unprecedented concurrent electro-optical mixing system is vigorous, well-founded, and reliable and can be interrogated with a variety of epochal and ubiquitous implementations.

Author Contributions: H.T. performed the principle, experiments, and simulations and prepared the manuscript; A.M. reviewed the manuscript. All authors have read and agreed to the published version of the manuscript.

Funding: This research received no external funding.

Institutional Review Board Statement: Not Applicable.

Informed Consent Statement: Not Applicable.

Data Availability Statement: Data underlying the results presented in this paper are not publicly available at this time but may be obtained from the authors upon reasonable request.

Conflicts of Interest: The authors declare no conflict of interest.

References

1. Kleine-Ostmann, T.; Nagatsuma, T. Review on Terahertz Communications Research. *J. Infrared Millim. Terahertz Waves* **2011**, *32*, 143–171. [CrossRef]
2. Gomes, N.J.; Monteiro, P.P.; Gameiro, A. *Next Generation Wireless Communications Using Radio over Fiber*; Wiley: West Sussex, UK, 2012.
3. Rouvalis, E.; Renaud, C.; Moodie, D.G.; Robertson, M.J.; Seeds, A.J. Traveling-wave Uni-Traveling Carrier Photodiodes for continuous wave THz generation. *Opt. Express* **2010**, *18*, 11105–11110. [CrossRef] [PubMed]
4. Preu, S.; Döhler, G.H.; Malzer, S.; Wang, L.J.; Gossard, A.C. Continuous-wave Terahertz photomixer sources and applications. *J. Appl. Phys* **2011**, *109*, 061301. [CrossRef]
5. Thomas, V.A.; El-Hajjar, M.; Hanzo, L. Millimeter-Wave Radio Over Fiber Optical Upconversion Techniques Relying on Link Nonlinearity. *IEEE Commun. Surv. Tutor.* **2016**, *18*, 29–53. [CrossRef]
6. Schilling, M.; Daub, K.; Idler, W.; Baums, D.; Koerner, U.; Lach, E.; Laube, G.; Wünstel, K. Wavelength converter based on integrated all-active three-port Mach- Zehnder interferometer. *Electron. Lett.* **1994**, *30*, 2128–2130. [CrossRef]
7. Dong, H.; Sun, H.; Wang, Q.; Dutta, N.K.; Jaques, J. All optical logic and operation at 80 Gb/s using semiconductor optical amplifier based on the Mach-Zehnder interferometer. *Microw. Opt. Technol. Lett.* **2006**, *48*, 1672–1675. [CrossRef]
8. Dimitriadou, E.; Zoiros, K.E. On the design of reconfigurable ultrafast all-optical NOR and NAND gates using a single quantum-dot semiconductor optical amplifier-based Mach- Zehnder interferometer. *J. Opt.* **2012**, *14*, 105401. [CrossRef]
9. Houbavlis, T.; Zoiros, K.E.; Kanellos, G.; Tsekrekos, C. Performance analysis of ultrafast all-optical Boolean XOR gate using semiconductor optical amplifier-based Mach-Zehnder Interferometer. *Opt. Commun.* **2004**, *232*, 179–199. [CrossRef]
10. Kim, S.H.; Kim, J.H.; Yu, B.G.; Byun, Y.T.; Jeon, Y.M.; Lee, S.; Woo, D.H. All-optical NAND gate using cross-gain modulation in semiconductor optical amplifiers. *Electron. Lett.* **2005**, *41*, 1027–1028. [CrossRef]
11. Dong, H.; Sun, H.; Wang, Q.; Dutta, N.K.; Jaques, J. 80 Gb/s All-optical logic AND operation using Mach-Zehnder interferometer with differential scheme. *Opt. Commun.* **2006**, *265*, 79–83. [CrossRef]
12. Lee, S.; Park, J.; Lee, K.; Eom, D.; Lee, S.; Kim, J.H. All-optical exclusive NOR logic gate using Mach-Zender Interferometer. *Jpn. J. Appl. Phys.* **2002**, *41*, 1155–1157. [CrossRef]
13. Kang, B.-K.; Kim, J.H.; Park, Y.H.; Lee, S.; Jhon, Y.M.; Woo, D.H.; Kim, S.H.; Park, S.-H. All-optical logic AND in a SOA-based Mach-Zehnder all-optical wavelength converter. In Proceedings of the 13th Laser and Electro-Optics Society, Rio Grande, TX, USA, 13–16 November 2000; Volume 1, pp. 117–118.
14. Pan, X.; Wiesenfeld, J.M.; Perino, J.S.; Koch, T.L.; Raybon, G.; Koren, U.; Chien, M.; Young, M.; Miller, B.I.; Burrus, C.A. Dynamic operation of a three-port, integrated Mach-Zehnder wavelength converter. *IEEE Photonics Technol. Lett.* **1995**, *7*, 995–997. [CrossRef] [PubMed]
15. Sun, H.; Wang, Q.; Dong, H.; Dutta, N.K. XOR performance of a quantum dot semiconductor optical amplifier based Mach-Zehnder interferometer. *Opt. Express* **2005**, *13*, 1892–1899. [CrossRef]
16. Wang, Q.; Zhu, G.; Chen, H.; Jaques, J.; Leuthold, J.; Piccirilli, A.; Dutta, N. Study of All-Optical XOR using Mach-Zehnder Interferometer and Differential Scheme. *IEEE J. Quantum Electron.* **2004**, *40*, 703–710. [CrossRef]
17. Termos, H.; Mansour, A. Real & Simulated QPSK Up-Converted Signals by a Sampling Method Using a Cascaded MZMs Link. *Photonics* **2022**, *9*, 34.
18. Chul, S.P.; Choong, K.; Chung, G.L.; Dong-Hwan, K.; Chang-Soo, P.A. photonic up-converter for a WDM radio-over-fiber system using cross-absorption modulation in an EAM. *IEEE Photonics Technol. Lett.* **2005**, *17*, 1950–1952. [CrossRef]
19. Thouras, J.; Benazet, B.; Leblond, H.; Aupetit-Berthelemot, C. Photonic radio frequency down-converter based on parallel electro-absorption modulators in Ku/Ku band for space applications. In Proceedings of the 2016 21st OptoElectronics and Communications Conference (OECC) Held Join, Niigata, Japan, 3–7 July 2016.

20. Mohammad, A.W.; Shams, H.; Liu, C.-P.; Graham, C.; Natrella, M.; Seeds, A.J.; Renaud, C.C. 60-GHz Transmission link using uni-traveling carrier photodiodes at the transmitter and the receiver. *J. Light. Technol.* **2018**, *36*, 4507–4513. [CrossRef]
21. Rouvalis, E.; Fice, M.; Renaud, C.; Seeds, A.J. Millimeter-Wave Optoelectronic Mixers Based on Uni-Traveling Carrier Photodiodes. *IEEE Trans. Microw. Theory Tech.* **2012**, *60*, 686–691. [CrossRef]
22. Termos, H.; Mansour, A. Quadrature amplitude modulation frequency up-and down-conversions using a positive-intrinsic-negative photodiode sampling mixer. *Opt. Eng.* **2022**, *61*, 096103. [CrossRef]
23. Kim, H.J.; Song, J.I. Simultaneous WDM RoF Signal Generation Utilizing an All-Optical Frequency Upconverter Based on FWM in a SOA. *IEEE Photonics Technol. Lett.* **2011**, *23*, 828–830.
24. Contestabile, G.; Presi, M.; Ciaramella, E. Multiple Wavelength Conversion for WDM Multicasting by FWM in an SOA. *IEEE Photonics Technol. Lett.* **2004**, *16*, 1775–1777. [CrossRef]
25. Seo, Y.K.; Choi, C.S.; Choi, W.Y. All-Optical Signal Up-Conversion for Radio-on-Fiber Applications Using Cross-Gain Modulation in Semiconductor Optical Amplifiers. *IEEE Photonics Technol. Lett.* **2002**, *14*, 1448–1450. [CrossRef]
26. Contestabile, G.; Maruta, A.; Sekiguchi, S.; Morito, K.; Sugawara, M.; Kitayama, K. 80 Gb/s Multicast Wavelength Conversion by XGM in a QDSOA. In Proceedings of the 36th European Conference and Exhibition on Optical Communication, Turin, Italy, 19–23 September 2010; pp. 1–3.
27. Song, H.J.; Lee, J.S.; Song, J.I. Signal Up-Conversion by Using a Cross-Phase Modulation in All-Optical SOA-MZI Wavelength Converter. *IEEE Photonics Technol. Lett.* **2004**, *16*, 593–595. [CrossRef]
28. Song, H.J.; Song, J.I. Simultaneous All-Optical Frequency Downconversion Technique Utilizing an SOA-MZI for WDM Radio Over Fiber (RoF) Applications. *J. Light. Technol.* **2006**, *24*, 3028–3034. [CrossRef]
29. Song, J.I.; Song, H.J. Simultaneous Frequency Conversion Technique Utilizing an SOA-MZI For Full-Duplex WDM Radio over Fiber Applications. *IEICE Trans. Electron.* **2007**, *E90-C*, 351–358. [CrossRef]
30. Kim, H.J.; Lee, S.H.; Song, J.I. Generation of a 100-GHz optical SSB signal using XPM-based all-optical frequency up-conversion in an SOAMZI. *Microw. Opt. Technol. Lett.* **2014**, *57*, 35–38. [CrossRef]
31. Kim, D.H.; Lee, J.Y.; Choi, H.J.; Song, I.J. All-optical single sideband frequency up conversion utilizing the XPM effect in an SOAMZI. *Opt. Express.* **2016**, *24*, 20309–20317. [CrossRef] [PubMed]
32. Termos, H.; Rampone, T.; Sharaiha, A.; Hamié, A.; Alaeddine, A. All-Optical Radiofrequency Sampling Mixer Based on a Semiconductor Optical Amplifier Mach–Zehnder Interferometer Using a Standard and a Differential Configuration. *J. Light. Technol.* **2016**, *34*, 4688–4695. [CrossRef]
33. Termos, H.; Rampone, T.; Sharaiha, A.; Hamié, A.; Alaeddine, A. Up and down frequency conversion of a QPSK signal by an all-optical radiofrequency sampling mixer based on a semiconductor optical amplifier Mach-Zehnder interferometer. In Proceedings of the 2015 International Topical Meeting on Microwave Photonics (MWP), Paphos, Cyprus, 25–29 October 2015; pp. 1–4.
34. Termos, H.; Rampone, T.; Sharaiha, A.; Hamié, A.; Alaeddine, A. OFDM signal up and down frequency conversions by a sampling method using a SOA-MZI. In Proceedings of the 2017 29th International Conference on Microelectronics (ICM), Beirut, Lebanon, 10–13 December 2017; pp. 1–5.
35. Termos, H.; Rampone, T.; Sharaiha, A. Sampling rate influence in up and down mixing of QPSK and OFDM signals using an SOA-MZI in a differential configuration. *Electron. Lett.* **2018**, *54*, 990–991. [CrossRef]
36. Termos, H.; Mansour, A.; Nasser, A. Simultaneous up- and down-frequency mixing based on a cascaded SOA-MZIs link. *Appl. Opt.* **2021**, *60*, 8336–8348. [CrossRef]
37. Termos, H.; Mansour, A.; Nasser, A. Simultaneous Up-Conversion Based on a Co- & Counter-Directions SOA-MZI Sampling Mixer with Standard & Differential Modulation Modes. *Photonics* **2022**, *9*, 109.
38. Termos, H.; Mansour, A. OFDM signal down frequency conversion based on a SOA-MZI sampling mixer using differential modulation and switching architectures. *Optik* **2021**, *245*, 167761. [CrossRef]
39. Termos, H.; Mansour, A. Sampling Parallel SOA-MZIs Configuration for All-Optical Simultaneous Frequency Down-Conversion. *Photonics* **2022**, *9*, 745. [CrossRef]
40. Termos, H.; Tharthar, A.; Mansour, A. All-Optical Simultaneous Frequency Metamorphose Con-tin-gent on a Three Parallel SOA-MZIs Copula. *Optics* **2022**, *9*, 745.
41. Termos, H. Study of Up and Down Conversion Technique by all Optical Sampling Based on a SOA-MZI. Ph.D. Dissertation, ED SICMA. University de Bretagne Occidentale, Brest, France, February 2017.
42. Fernandez, A.; Chao, L.; Chi, J.W.D. All-optical clock recovery and pulse reshaping using semiconductor optical amplifier and dispersion compensating fiber in a ring cavity. *IEEE Photonics Technol. Lett.* **2008**, *20*, 1148–1150. [CrossRef]
43. Stasyuk, V. Test Data and Operation Manual of Ultrafast Optical Clock. Available online: www.pritel.com (accessed on 4 March 2023).
44. Capmany, J.; Sales, S.; Pastor, D.; Ortega, B. Optical mixing of microwave signals in a nonlinear semiconductor laser amplifier modulator. *Opt. Express* **2002**, *10*, 183–189. [CrossRef]
45. Bohe, C.; Sharaiha, A.; Khaleghi, T.R. Electro-optical radiofrequency mixer based on semiconductor optical amplifier, H. *Electron. Lett.* **2011**, *47*, 331–333.

46. Rampone, T.; Zulma, R. Electro-optical radiofrequency up-converter based on a semiconductor optical amplifier. In Proceedings of the 2011 International Topical Meeting on Microwave Photonics Jointly Held with the 2011 Asia-Pacific Microwave Photonics Conference, Singapore, 18–21 October 2011; Volume 31, pp. 145–148.
47. Termos, H.; Mansour, A. Frequency Alteration Built on an Electro-Optical Sampling SOA–MZI Using a Differential Modulation Schema. *Optics* **2022**, *3*, 225–233. [CrossRef]
48. Vaughan, R.G.; Scott, N.L.; White, D.R. The theory of band pass sampling. *IEEE Trans. Signal Process.* **1991**, *39*, 1973–1984. [CrossRef]
49. Runge, P.; Bunge, C.A.; Petermann, K. All-Optical Wavelength Conversion with Extinction Ratio Improvement of 100 Gb/s RZ-Signals in Ultralong Bulk Semiconductor Optical Amplifiers. *IEEE J. Quantum Electron.* **2010**, *46*, 937–944. [CrossRef]
50. Leuthold, J.; Marom, D.M.; Cabot, S.; Jaques, J.J.; Ryf, R.; Giles, C.R. All-optical wavelength conversion using a pulse reformatting optical filter. *J. Light. Technol.* **2004**, *22*, 186–192. [CrossRef]
51. Liu, Y.; Tangdiongga, E.; Li, Z.; De Waardt, H.; Koonen, A.M.; Khoe, G.D.; Dorren, H.J.; Shu, X.; Bennion, I. Error-free 320 Fb/s SOA-Based Wavelength Conversion Using Optical Filtering. In Proceedings of the 2006 Optical Fiber Communication Conference and the National Fiber Optic Engineers Conference, Anaheim, CA, USA, 5–10 March 2006.
52. Spyropoulou, M.; Pleros, N.; Miliou, A. SOA-MZI-based nonlinear optical signal processing: A frequency domain transfer function for wavelength conversion, clock recovery, and packet envelope detection. *IEEE J. Quantum Electron.* **2010**, *47*, 40–49. [CrossRef]
53. Termos, H.; Mansour, A.; Ebrahim-Zadeh, M. Establishment of an Electro-Optical Mixing Design on a Photonic SOA-MZI Using a Differential Modulation Arrangement. *Sensors* **2023**, *23*, 4380. [CrossRef]
54. Maker, V.P.T.; Manual, U. Photonic Modules Reference Manuals. VPI Photonics Official Website. Available online: http://www.vpiphotonics.com (accessed on 1 February 2023).
55. Ito, H.; Furuta, T.; Kodama, S.; Ishibashi, T. InP/InGaAs uni-travelling-carrier photodiode with 310 GHz bandwidth. *Electron. Lett.* **2000**, *36*, 1809–1810. [CrossRef]
56. Rouvalis, E.; Fice, M.J.; Renaud, C.C.; Seeds, A.J. Optoelectronic detection of millimeter-wave signals with travelling-wave uni-travelling carrier photodiodes. *Opt. Express* **2011**, *19*, 2079–2084. [CrossRef]
57. Shafik, R.A.; Rahman, S.; Islam, A.R. On the Extended Relationships among EVM, BER and SNR as Performance Metrics. In Proceedings of the 2006 International Conference on Electrical and Computer Engineering, Dhaka, Bangladesh, 19–21 December 2006; pp. 408–411.
58. Agrawal, G.P. *Fiber-Optic Communications Systems*; Wiley: New York, NY, USA, 1997.
59. Walker, G.; Steele, R.; Walker, N. Optical amplifier noise figure in a coherent optical transmission system. *J. Light. Technol.* **2002**, *8*, 1409–1413. [CrossRef]
60. Crottini, A.; Salleras, F.; Moreno, P.; Dupertuis, M.A.; Deveaud, B.; Brenot, R. Noise Figure Improvement in Semiconductor Optical Amplifiers by Holding Beam at Transparency Scheme. *IEEE Photonics Technol. Lett.* **2005**, *17*, 977–979. [CrossRef]
61. Picard, R.B.; Alouini, M.; Lopez, J.; Vodjdani, N.; Simon, J.-C. Impact of the Gain Saturation Dynamics in Semiconductor Optical Amplifiers on the Characteristics of an Analog Optical Link. *J. Light. Technol.* **2005**, *23*, 2420–2426. [CrossRef]
62. Eriksson, P.; Tenhunen, H. The noise figure of a sampling mixer: Theory and measurement. In Proceedings of the ICECS'99 6th IEEE International Conference on Electronics, Circuits and Systems, Paphos, Cyprus, 5–8 September 1999; Volume 2, pp. 899–902.
63. Movassaghi, M.; Jackson, M.K.; Smith, V.M.; Young, J.F.; Hallam, W.J. Noise figure of saturated erbium-doped fiber amplifiers. In Proceedings of the Optical Fiber Communication Conference, Dallas, TX, USA, 16–21 February 1997; Volume 6, pp. 104–105.
64. Baney, D.M.; Jungerman, R.L. Optical Noise Standard for the Electrical Method of Optical Amplifier Noise Figure Measurement. In *Optical Amplifiers and Their Applications*; Optical Society of America: Washington, WA, USA, 1997.
65. Razavi, B. Design considerations for direct-conversion receivers. *IEEE Trans. Circuits Syst.* **1997**, *44*, 428–435. [CrossRef]
66. Nelson, C.W.; Hati, A.; Howe, D.A. A collapse of the cross-spectral function in phase noise metrology. *Rev. Sci. Instrum.* **2014**, *85*, 024705. [CrossRef]
67. Grove, J.; Hein, J.; Retta, J.; Schweiger, P.; Solbrig, W.; Stein, S.R. Direct-digital phase-noise measurement. In Proceedings of the 2004 IEEE International Frequency Control Symposium and Exposition, Montreal, QC, Canada, 23–27 August 2004; pp. 287–291.
68. Parker, S.R.; Ivanov, E.N.; Hartnett, J.G. Extending the Frequency Range of Digital Noise Measurements to the Microwave Domain. *IEEE Trans. Microw. Theory Tech.* **2014**, *62*, 368–372. [CrossRef]
69. ARMStrong, J. OFDM for Optical Communications. *J. Light. Technol.* **2009**, *27*, 189–204. [CrossRef]
70. Schmogrow, R.; Nebendahl, B.; Winter, M.; Josten, A.; Hillerkuss, D.; Koenig, S.; Meyer, J.; Dreschmann, M.; Huebner, M.; Koos, C.; et al. Error Vector Magnitude as a Performance Measure for Advanced Modulation Formats. *IEEE Photonics Technol. Lett.* **2011**, *24*, 61–63. [CrossRef]
71. Mestre, M.A.; Mardoyan, H.; Caillaud, C.; Rios-Müller, R.; Renaudier, J.; Jennevé, P.; Blache, F.; Pommereau, F.; Decobert, J.; Jorge, F. Compact InP-based DFB-EAM enabling PAM-4 112 Gb/s transmission over 2 km. *J. Light. Technol.* **2016**, *34*, 1572–1578. [CrossRef]
72. Li, G.; Li, J.Q.; Chen, G.J.; Huang, X.G. SOA-based AOWC of 128-QAM Using Gaussian Pulse Shaping for Transmission System with 227 Gbps. *Microw. Opt. Technol. Lett.* **2018**, *60*, 2204–2216. [CrossRef]

Disclaimer/Publisher's Note: The statements, opinions and data contained in all publications are solely those of the individual author(s) and contributor(s) and not of MDPI and/or the editor(s). MDPI and/or the editor(s) disclaim responsibility for any injury to people or property resulting from any ideas, methods, instructions or products referred to in the content.